Ultrafast electron diffraction using an ultracold source

Ultrafast electron diffraction using an ultracold source

M. W. van Mourik, W. J. Engelen, E. J. D. Vredenbregt, and O. J. Luiten

Citation: Structural Dynamics **1**, 034302 (2014); doi: 10.1063/1.4882074
View online: http://dx.doi.org/10.1063/1.4882074
View Table of Contents: http://scitation.aip.org/content/aca/journal/sdy/1/3?ver=pdfcov
Published by the American Crystallographic Association, Inc.

Ultrafast electron diffraction using an ultracold source

M. W. van Mourik,[1] W. J. Engelen,[1] E. J. D. Vredenbregt,[1,2] and O. J. Luiten[1,2]
[1]*Department of Applied Physics, Eindhoven University of Technology, P.O. Box 513, 5600 MB Eindhoven, The Netherlands*
[2]*Institute for Complex Molecular Systems, Eindhoven University of Technology, P.O. Box 513, 5600 MB Eindhoven, The Netherlands*

(Received 24 April 2014; accepted 27 May 2014; published online 6 June 2014)

The study of structural dynamics of complex macromolecular crystals using electrons requires bunches of sufficient coherence and charge. We present diffraction patterns from graphite, obtained with bunches from an ultracold electron source, based on femtosecond near-threshold photoionization of a laser-cooled atomic gas. By varying the photoionization wavelength, we change the effective source temperature from 300 K to 10 K, resulting in a concomitant change in the width of the diffraction peaks, which is consistent with independently measured source parameters. This constitutes a direct measurement of the beam coherence of this ultracold source and confirms its suitability for protein crystal diffraction. [http://dx.doi.org/10.1063/1.4882074]

I. INTRODUCTION

The fast pace at which the field of ultrafast structural dynamics is currently evolving is largely due to spectacular developments in ultrafast X-ray[1–3] and electron[4–6] beams. A particularly interesting development is the ultracold electron source, which is based on near-threshold photo-ionization of a laser-cooled and trapped atomic gas.[7–11] Recently, it was shown that the ultracold electron source can be operated at femtosecond timescales while, surprisingly, retaining its high spatial coherence.[10,11]

Typical ultrafast electron diffraction (UED) experiments are performed using a planar photocathode source,[4] characterized by effective electron temperatures $T \geq 1000$ K. These temperatures can, to a certain degree, be controlled by adjusting the photoemission laser wavelength.[12,13] Kirchner *et al.*[14] have shown that by focusing the femtosecond photoemission laser to a small spot on a gold cathode and extracting not more than a single electron per pulse, a root-mean-square (rms) source size of $\sigma_{\text{source}} = 3\,\mu$m can be achieved. In combination with a rms beam size at the sample of $\sigma_{\text{sample}} = 77\,\mu$m, this results in transverse coherence lengths of

$$L_\perp \equiv \frac{\hbar}{\sigma_{p_\perp}} = \frac{\hbar}{\sqrt{m k_B T}} \frac{\sigma_{\text{sample}}}{\sigma_{\text{source}}} \approx 20\,\text{nm}, \tag{1}$$

with $\hbar$ being the Dirac's constant, $\sigma_{p_\perp}$ being the rms transverse momentum, m being the electron mass, and k_B being the Boltzmann's constant. To resolve a diffraction pattern, $L_\perp$ should be larger than the lattice constant a of the sample under investigation. A coherence length of $L_\perp = 20$ nm is more than sufficient for protein crystal diffraction (with typically $a = 1$–5 nm), as shown in Ref. 14 on an organic salt with $a \approx 1$ nm. An even larger coherence length can be achievable by extracting single electrons from tip-based sources.[15] For a full, high-quality diffraction pattern of a complicated macromolecular crystal, 10^6–10^7 electrons are required. Measurements using single-electron pulses are therefore restricted to processes which can be repeated reproducibly millions of times. This is particularly important when studying samples

susceptible to pump laser damage.[4] An ultrafast electron source producing more charge per pulse but with the same beam quality is therefore highly desirable.

The ultracold electron source has been developed as an alternative candidate for ultrafast electron diffraction, providing the required higher beam brightness. The source was previously shown to have effective temperatures as low as 10 K,[9,10] implying a coherence length at least an order of magnitude larger compared to conventional photocathodes, for similar source sizes and charges. Alternatively, the ultracold source can be operated with a source size an order of magnitude larger than that of photocathodes, while achieving the same coherence length. This allows extraction of at least 100 times more charge per pulse. So far, the beam properties of the ultracold and ultrafast source have been studied, but the source has not yet been applied for imaging or diffraction.

Here, we present diffraction patterns of a mono-crystalline graphite sample generated with picosecond electron bunches extracted from an ultracold source. We achieve sharp diffraction spots by focusing the beam through the sample onto the detector. When focusing the beam to a micron-sized spot on the sample, diffraction spots expand considerably but remain clearly distinguishable. The enlarged diffraction spot sizes allow us to directly determine the coherence properties of the beam at the sample, which we find to be consistent with independently measured source parameters.

II. EXPERIMENTAL SET-UP

Fig. 1 shows a schematic overview of the set-up, which is described in more detail in Refs. 16 and 17. Electrons are created by near-threshold photoionization of a laser-cooled and trapped cloud of ^{85}Rb atoms. Rubidium atoms are first excited from the 5s to the 5p state and subsequently ionized by a ≈100 fs full-width-at-half-maximum long laser pulse with a tunable central wavelength λ_l (Fig. 1(a)). The excitation and ionization laser pulses propagate along perpendicular directions (Fig. 1(b)) and overlap in a well-defined region within the magneto-optical trap (MOT), resulting in an ionized cloud a few tens of microns in size in all three directions.

Typically, a few hundred electrons are produced per shot. The laser-cooled gas cloud is trapped inside an accelerator structure (Fig. 1(b)) with local electric field strength F. The combination of λ_l and F determines the kinetic energy distribution of the released electrons, and thus the effective source temperature T.[17] The thermal energy k_BT is on the order of the excess energy of the electrons, which is given by

$$E_{\mathrm{exc}} = 2\pi\hbar c\left(\frac{1}{\lambda_l} - \frac{1}{\lambda_0}\right) + 2E_h\sqrt{\frac{F}{F_0}}, \tag{2}$$

with c being the speed of light, $\lambda_0 = 479.06$ nm, the zero-field ionization threshold wavelength, $E_h = 27.2$ eV being the Hartree energy, and $F_0 = 5.14 \times 10^{11}$ V/m being the atomic unit of field strength. Electrons are extracted from the cloud by the electric field and are accelerated to a final energy $U = eFd_{\mathrm{acc}}$, with e being the elementary charge, and $d_{\mathrm{acc}} = 12.7$ mm.

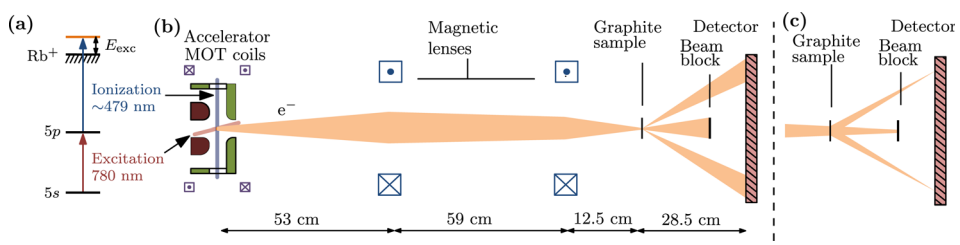

FIG. 1. Experimental set-up. (a) Magneto-optically trapped atoms are ionized by two perpendicular laser beams via a two step ionization scheme. Electrons are first excited from the 5*s* to the 5*p* state, and subsequently ionized. (b) The electron bunch is accelerated towards a detector. A set of magnetic lenses controls the beam divergence and size, allowing us to focus the beam on the sample (b) or on the detector (c). The beam passes through a graphite sample and undergoes diffraction. The 0th order beam is blocked.

At 1.245 m from the source, the beam is sent through a 13–20 nm thick monocrystalline graphite sample[18] on a 200 mesh copper TEM grid. At a distance of $h = 0.285$ m from the sample, electrons arrive at a microchannel plate with phosphor screen, imaged by a CCD camera. Two magnetic lenses (at 0.53 m and 1.12 m) provide control over the spot size and the angular spread of the beam on the sample. To obtain sharp diffraction patterns, we focus the beam on the detector, resulting in a converging beam with a rms size of $\sigma_{\text{sample}} \sim 200\ \mu$m at the sample, schematically shown in Fig. 1(c). Alternatively, we can focus the beam to a micron-sized beam on the sample, as shown in Fig. 1(b), allowing us to analyze the quality of diffraction spots more conveniently.

III. SOURCE PARAMETERS

According to Eq. (1), the coherence length of the beam is dependent on the source size σ_{source} and the effective source temperature T. The source size is determined by means of an ion space charge scan, in which the spot size of an ion bunch is measured at the detector as a function of bunch charge.[17] The spot size is partly determined by the repulsive effects of space charge. Ions are used instead of electrons primarily because the former is negligibly heated during the ionization process, so that angular spread due to temperature can be ignored. We scan through the bunch charge by changing the intensity of the ionization laser pulse using neutral density (ND) filters. Fig. 2(a) shows the result of a space charge scan. The resulting spot sizes (green triangles and blue squares) are compared to particle tracking simulations using the General Particle Tracer (GPT) code[19] (dotted lines), which calculates charged particle trajectories through known electric and magnetic fields.[8,17] In the simulations, both the initial source size in two directions, σ_{source}, $\{x, y\}$, and a proportionality factor between laser intensity and bunch charge are varied. The best overlap between experimental and simulation data in the least-squares sense, as shown in the inset, is obtained for initial source size, σ_{source}, $x(y) = 32 \pm 2(54 \pm 2)\ \mu$m. Throughout this paper, the dimensions x and y refer to the transverse minor and major axes, respectively, of the charged particle beam which is generally elliptically shaped.

Using the waist scan method, the thermal emittance $\epsilon_{\text{th}} \equiv \sigma_{\text{source}} \sqrt{\frac{k_B T}{mc^2}}$ of the source can be determined,[17] which, combined with σ_{source}, yields the effective source temperature T. In a waist scan, the current of a magnetic solenoid lens halfway the beam line is altered, changing the beam spot size on the detector. From the dependence of the spot size on the focusing strength, the source emittance (and thus temperature) is determined. We have established that for $F = 0.85$ MV/m the source temperature T can be varied from 300 K to 10 K by tuning λ_l from 477 nm to 500 nm, displayed in Fig. 2(b). Consequently, the emittance of the beam is varied from $\epsilon_{\text{th},x(y)} = 7.2\ (12.2)$ nm rad to 1.3 (2.2) nm rad.

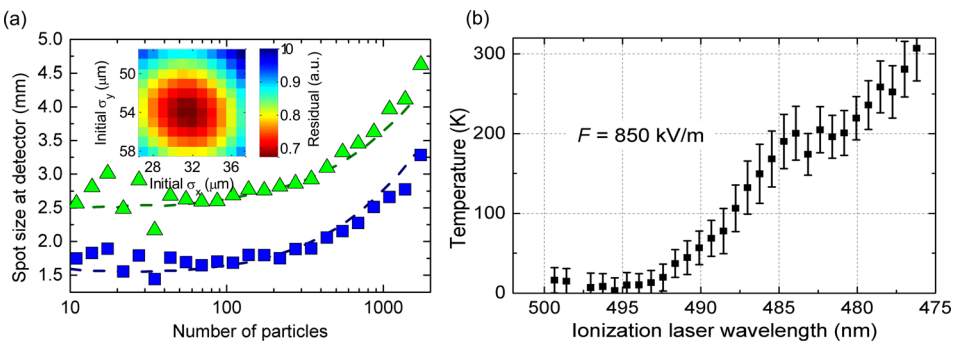

FIG. 2. Source parameters. (a) Results of an ion space charge scan to determine σ_{source}. The spot size at the detector, in two directions (green triangles and blue squares) is shown as function of bunch charge. The inset shows the normalized residual between experimental and simulation data for various simulated source sizes. From this, we determine the source size is $\sigma_{\text{source},x} \times \sigma_{\text{source},y} = (32 \pm 2) \times (54 \pm 2)\ \mu\text{m}^2$. The dotted lines indicate the simulated final spot sizes as a function of bunch charge for the best fit. (b) Effective transverse source temperature as function of ionization laser wavelength, determined using waist scans for an electric field strength of $F = 850$ kV/m. For large wavelengths, temperatures reach $T \approx 10$ K. The uncertainty of the data points is partly due to a systematic error in fitting a waist scan.

IV. RESULTS

To record a single diffraction pattern, 10^3 shots are acquired at a 100 Hz repetition rate. Each shot contains a few hundred electrons. We have checked that for such bunch charges space charge effects are negligible, which are confirmed by charged particle tracking simulations.

Fig. 3(a) shows an electron diffraction pattern produced with the beam focused onto the detector (Fig. 1(c)), using only the first magnetic lens. For illustrative purposes, the diffraction pattern shown here is an average over 10 images. The pattern was recorded with beam parameters $U = 13.2$ keV and $\lambda_l = 485$ nm.

Five of the six 1st order spots (1) of the expected hexagonal pattern are visible, centered around the beam block (3). The sixth 1st order spot is blocked by the stem of the beam block. In the bottom left, a 2nd order spot (2) can be seen; the others fall outside the detection area (4). The 1st order beamlets arrive at the detector at a distance of $s = 14.3$ mm from the central (0th order) beam. The 1st order diffraction angle is $\theta = \tan^{-1}(s/h) = 50 \pm 1$ mrad, in agreement with the theoretical value from Bragg's law, $\theta_B = 49.9$ mrad.

The rms spot size on the detector (magnified and profiled in Fig. 3(b)) is measured to be $\sigma_{d,x(y)} = 180$ (210) μm. The size σ_d of the diffraction spot is actually expected to be as low as 30 μm, on the basis of measured source temperature and size, but is limited by the detector resolution and beam instabilities.

To unambiguously demonstrate the full quality of the beam, without being limited by detector resolution or beam instability, measurements have been done with the beam focused to micron-sized spots on the sample (Fig. 1(b)). In this configuration, diffraction spots expand to a much larger size, but remain clearly distinguishable. For an electron energy $U = 10.8$ keV, diffraction images have been taken for ionization laser wavelengths $\lambda_l = 500$–477 nm ($T \approx 10$–300 K). Complementary to our experimental data, we simulate the beam properties using GPT, from which we find a spot size on the sample $\sigma_{sample} = 3.3$ μm for 10 K and $\sigma_{sample} = 8.7$ μm for 250 K.

Figs. 3(c) and 3(e) show two examples of diffraction images from this data set, at ionization laser wavelengths of 478 and 498 nm, respectively, corresponding to measured source

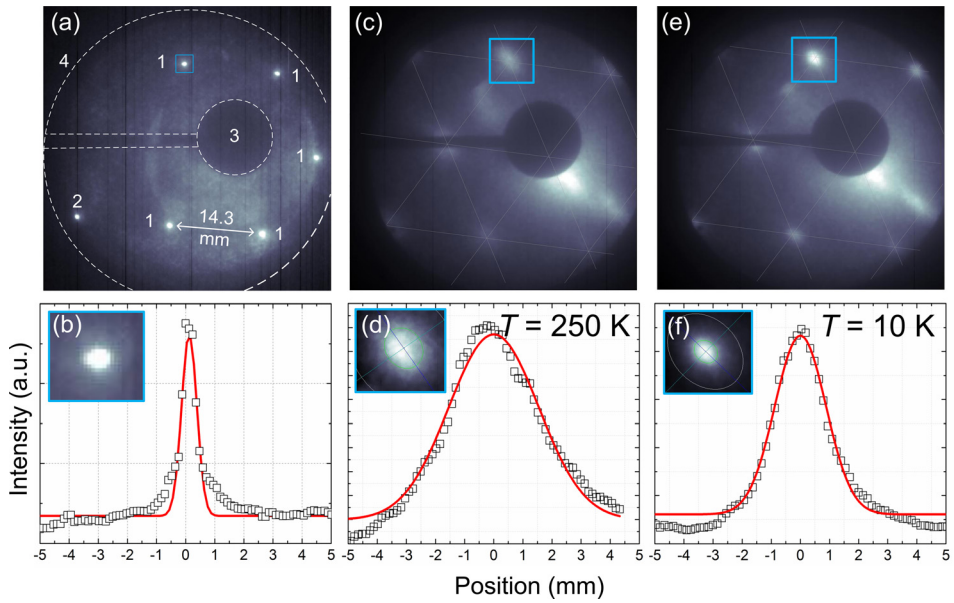

FIG. 3. Diffraction images obtained with the ultracold source (a) 13.2 keV electrons are focused on the detector using the first magnetic lens. Five 1st order spots (1) and one 2nd order spot (2) are visible. The intraspot distance is 14.3 mm. The beam block (3) and detector edge (4) are outlined. (b) shows the line profile along the minor axis of one of the spots and its Gaussian fit, from which spot size is determined. (c) and (e) show diffraction images obtained with a 10.8 keV beam focused on the sample, for source temperatures of $T = 250$ K (c) and $T = 10$ K (e). The improved beam quality due to lower temperatures can be seen by comparing close-up views of a spot and the respective line profiles (d) and (f) of their minor axes.

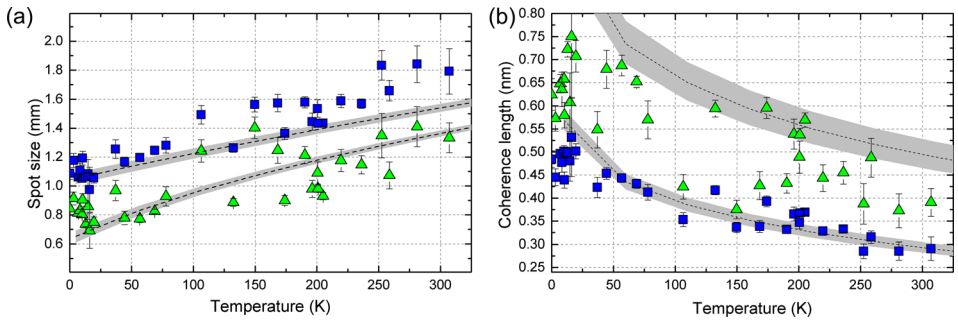

FIG. 4. (a) Final diffraction spot size σ_d as a function of effective source temperatures. The two data sets (green triangles and blue squares) are diffraction spot sizes determined using a 2-dimensional Gaussian fit of the elliptical diffraction spots. The gray bands are simulated spot sizes. (b) Coherence length, calculated from σ_d measurements, using Eq. (3). The gray bands are coherence lengths determined using source parameters and the GPT simulated beam size at the sample (Eq. (1)).

temperatures of $T = 250$ and 10 K. The thin gray lines are guides to show the hexagonal diffraction pattern. The spots inside the blue squares have been magnified and profiled in (d) ($T = 250$ K) and (f) ($T = 10$ K). Two-dimensional Gaussian fits are used to determine the size of the spots: $\sigma_{d,x(y)} = 1.6$ (1.8) mm for $T = 250$ K and $\sigma_{d,x(y)} = 0.88$ (1.1) mm for $T = 10$ K. The diffraction spots clearly become sharper when lowering the source temperature.

The diffraction spot sizes σ_d are plotted as function of source temperature in Fig. 4(a), where the two sets represent the rms sizes of the minor (green triangles) and major (blue squares) axes of the elliptical spots. Each individual data point is the average over spot sizes obtained from 10 diffraction images. The results are in general agreement with the values from GPT simulations (black line ± shaded area). This shows that the spot sizes of the diffraction patterns behave as expected on the basis of source properties. The scatter in the data points is attributed to pointing instabilities in the femtosecond ionization laser, which cause the position and size of the ionization volume, thus the final spot size, to vary.

It is instructive to discuss the results shown in Fig. 4(a) in terms of coherence length. Writing the coherence length in terms of angular spread σ_θ of the beam, $L_\perp = \frac{\hbar}{\sigma_\theta\sqrt{2mU}}$, and the kinetic energy U in terms of the diffraction angle from Bragg's law, $\sqrt{U} = \frac{2\pi\hbar}{a_1\theta\sqrt{2m}}$, with $a_1 = 0.2131$ nm graphite's first order lattice constant, we find $L_\perp = a_1\theta/2\pi\sigma_\theta$. Since $\sigma_{sample} \ll \sigma_d$, σ_d is dominated by the angular spread of the beam. This allows us to write $L_\perp$ as

$$L_\perp \approx \frac{a_1 s}{2\pi\sigma_d}, \tag{3}$$

implying that $L_\perp$ can be determined directly from diffraction data, independent of the source parameters.

Fig. 4(b) shows the coherence lengths as a function of source temperature, determined using Eq. (3) and the data shown in Fig. 4(a). As expected, the measured coherence length increases when lowering the source temperature. The gray bands in Fig. 4(b) are coherence lengths calculated using Eq. (1) with the measured source parameters and σ_{sample} from GPT simulations. From the similarity between the experimental and simulated coherence lengths, we conclude that the values of $L_\perp$ calculated using Eq. (3) are consistent with Eq. (1). This shows that the quality of the diffraction pattern agrees with emittance of the beam as determined from the source properties.

V. CONCLUSION

In conclusion, we have shown that the ultracold electron source is capable of producing sharp diffraction patterns of mono-crystalline graphite. When focusing the beam down to a micron-sized spot on the sample, we find that the enlarged diffraction spots remain distinguishable, which is a consequence of the low source temperature. In this situation, we can accurately analyze the diffraction spots, from which the beam's coherence length $L_\perp$ at the sample is

directly determined, and is found to be consistent with independently measured source characteristics. The data from Fig. 4(b) and Eq. (1) together imply that with a sample size of 100 μm, a coherence length of at least 15 nm is reachable, with a few 100 electrons per pulse.

Actually, much more charge, up to a few times 10^4 electrons, can be extracted from the same ionization volume, given the local atomic density. However, this will significantly reduce the beam's coherence length through space-charge effects.[9,20] Developing methods to manage, and to a certain degree undo, space-charge effects[21,22] then becomes necessary to preserve the beam brightness. That would represent the next step towards single-shot ultrafast electron diffraction for the study of structural dynamics of complex molecular crystals.

ACKNOWLEDGMENTS

The authors wish to thank E. Rietman, I. Koole, and H. van Doorn for technical support. This research was supported by the Dutch Technology Foundation STW, Applied Science Division of NWO, and the Technology Programme of the Ministry of Economic Affairs.

[1]P. Emma, R. Akre, J. Arthur, R. Bionta, J. Bostedt, C. Bostedt, A. Brachmann, P. Bucksbaum, R. Coffee, F.-J. Decker, Y. Ding, D. Dowell, S. Edstrom, A. Fisher, J. Frisch, S. Gilevich, J. Hastings, G. Hays, P. Hering, Z. Huang, R. Iverson, H. Loos, M. Messerschmidt, A. Miahnahri, S. Moeller, H.-D. Nuhn, G. Pile, D. Ratner, J. Rzepiela, D. Schultz, T. Smith, P. Stefan, H. Tompkins, J. Turner, J. Welch, W. White, J. Wu, G. Yocky, and J. Galayda, "First lasing and operation of an angstrom-wavelength free-electron laser," Nat. Photonics **4**, 641–647 (2010).

[2]H. N. Chapman, P. Fromme, A. Barty, T. A. White, R. A. Kirian, A. Aquila, M. S. Hunter, J. Schulz, D. P. DePonte, U. Weierstall, R. B. Doak, F. R. N. C. Maia, A. V. Martin, I. Schlichting, L. Lomb, N. Coppola, R. L. Shoeman, S. W. Epp, R. Hartmann, D. Rolles, A. Rudenko, L. Foucar, N. Kimmel, G. Weidenspointner, P. Holl, M. Liang, M. Barthelmess, C. Caleman, S. Boutet, M. J. Bogan, J. Krzywinski, C. Bostedt, S. Bajt, L. Gumprecht, B. Rudek, B. Erk, C. Schmidt, A. Homke, C. Reich, D. Pietschner, L. Struder, G. Hauser, H. Gorke, J. Ullrich, S. Herrmann, G. Schaller, F. Schopper, H. Soltau, K.-U. Kuhnel, M. Messerschmidt, J. D. Bozek, S. P. Hau-Riege, M. Frank, C. Y. Hampton, R. G. Sierra, D. Starodub, G. J. Williams, J. Hajdu, N. Timneanu, M. M. Seibert, J. Andreasson, A. Rocker, O. Jonsson, M. Svenda, S. Stern, K. Nass, R. Andritschke, C.-D. Schroter, F. Krasniqi, M. Bott, K. E. Schmidt, X. Wang, I. Grotjohann, J. M. Holton, T. R. M. Barends, R. Neutze, S. Marchesini, R. Fromme, S. Schorb, D. Rupp, M. Adolph, T. Gorkhover, I. Andersson, H. Hirsemann, G. Potdevin, H. Graafsma, B. Nilsson, and J. C. H. Spence, "Femtosecond X-ray protein nanocrystallography," Nature **470**, 73–77 (2011).

[3]S. Boutet, L. Lomb, G. J. Williams, T. R. M. Barends, A. Aquila, R. B. Doak, U. Weierstall, D. P. DePonte, J. Steinbrener, R. L. Shoeman, M. Messerschmidt, A. Barty, T. A. White, S. Kassemeyer, R. A. Kirian, M. M. Seibert, P. A. Montanez, C. Kenney, R. Herbst, P. Hart, J. Pines, G. Haller, S. M. Gruner, H. T. Philipp, M. W. Tate, M. Hromalik, L. J. Koerner, N. van Bakel, J. Morse, W. Ghonsalves, D. Arnlund, M. J. Bogan, C. Caleman, R. Fromme, C. Y. Hampton, M. S. Hunter, L. C. Johansson, G. Katona, C. Kupitz, M. Liang, A. V. Martin, K. Nass, L. Redecke, F. Stellato, N. Timneanu, D. Wang, N. A. Zatsepin, D. Schafer, J. Defever, R. Neutze, P. Fromme, J. C. H. Spence, H. N. Chapman, and I. Schlichting, "High-resolution protein structure determination by serial femtosecond crystallography," Science **337**, 362–364 (2012).

[4]G. Sciaini and R. J. D. Miller, "Femtosecond electron diffraction: heralding the era of atomically resolved dynamics," Rep. Prog. Phys. **74**, 096101 (2011).

[5]M. Chergui and A. H. Zewail, "Electron and X-ray methods of ultrafast structural dynamics: Advances and applications," ChemPhysChem **10**, 28–43 (2009).

[6]M. Gao, C. Lu, H. Jean-Ruel, L. C. Liu, A. Marx, K. Onda, S.-y. Koshihara, Y. Nakano, X. Shao, T. Hiramatsu, G. Saito, H. Yamochi, R. R. Cooney, G. Moriena, G. Sciaini, and R. J. D. Miller, "Mapping molecular motions leading to charge delocalization with ultrabright electrons," Nature **496**, 343–346 (2013).

[7]B. J. Claessens, S. B. van der Geer, G. Taban, E. J. D. Vredenbregt, and O. J. Luiten, "Ultracold electron source," Phys. Rev. Lett. **95**, 164801 (2005).

[8]G. Taban, M. P. Reijnders, B. Fleskens, S. B. van der Geer, O. J. Luiten, and E. J. D. Vredenbregt, "Ultracold electron source for single-shot diffraction studies," Europhys. Lett. **91**, 46004 (2010).

[9]A. J. McCulloch, D. V. Sheludko, S. D. Saliba, S. C. Bell, M. Junker, K. A. Nugent, and R. E. Scholten, "Arbitrarily shaped high-coherence electron bunches from cold atoms," Nat. Phys. **7**, 785–789 (2011).

[10]W. J. Engelen, M. A. van der Heijden, D. J. Bakker, E. J. D. Vredenbregt, and O. J. Luiten, "High-coherence electron bunches produced by femtosecond photoionization," Nat. Commun. **4**, 1693 (2013).

[11]A. J. McCulloch, D. V. Sheludko, M. Junker, and R. E. Scholten, "High-coherence picosecond electron bunches from cold atoms," Nat. Commun. **4**, 1692 (2013).

[12]M. Aidelsburger, F. O. Kirchner, F. Krausz, and P. Baum, "Single-electron pulses for ultrafast diffraction," Proc. Natl. Acad. Sci. U.S.A. **107**, 19714–19719 (2010).

[13]C. P. Hauri, R. Ganter, F. Le Pimpec, A. Trisorio, C. Ruchert, and H. H. Braun, "Intrinsic emittance reduction of an electron beam from metal photocathodes," Phys. Rev. Lett. **104**, 234802 (2010).

[14]F. O. Kirchner, S. Lahme, F. Krausz, and P. Baum, "Coherence of femtosecond single electrons exceeds biomolecular dimensions," New J. Phys. **15**, 063021 (2013).

[15]J. Hoffrogge, J. Paul Stein, M. Krüger, M. Förster, J. Hammer, D. Ehberger, P. Baum, and P. Hommelhoff, "Tip-based source of femtosecond electron pulses at 30 keV," J. Appl. Phys. **115**, 094506 (2014).

[16]G. Taban, M. P. Reijnders, S. C. Bell, S. B. van der Geer, O. J. Luiten, and E. J. D. Vredenbregt, "Design and validation of an accelerator for an ultracold electron source," Phys. Rev. Spec. Top. -Accel. Beams **11**, 050102 (2008).

[17]W. Engelen, E. Smakman, D. Bakker, O. Luiten, and E. Vredenbregt, "Effective temperature of an ultracold electron source based on near-threshold photoionization," Ultramicroscopy **136**, 73–80 (2014).
[18]Sample produced by mechanical exfoliation of Naturally Graphite sample, see http://graphitecrystals.com.
[19]S. B. Van der Geer and M. J. De Loos, "General Particle Tracer" (2011), see www.pulsar.nl/gpt.
[20]S. B. van der Geer, M. J. de Loos, E. J. D. Vredenbregt, and O. J. Luiten, "Ultracold electron source for single-shot, ultrafast electron diffraction," Microsc. Microanal. **15**, 282–289 (2009).
[21]B. Carlsten, "New photoelectric injector design for the Los Alamos National Laboratory XUV FEL accelerator," Nucl. Instrum. Methods Phys. Res., Sect. A **285**, 313–319 (1989).
[22]L. Serafini and J. B. Rosenzweig, "Envelope analysis of intense relativistic quasilaminar beams in rf photoinjectors: A theory of emittance compensation," Phys. Rev. E **55**, 7565–7590 (1997).